Operation of the second-harmonic magnetic modulator with sinusoidal and square wave excitation voltages

Saad, I. M. H.

Report (National Research Council of Canada. Radio and Electrical Engineering Division : ERB), 1970-03

ERB-838

UNCLASSIFIED

NATIONAL RESEARCH COUNCIL OF CANADA

RADIO AND ELECTRICAL ENGINEERING DIVISION

OPERATION OF THE SECOND-HARMONIC MAGNETIC MODULATOR WITH SINUSOIDAL AND SQUARE WAVE EXCITATION VOLTAGES

- I. M. H. SAAD -

OTTAWA

MARCH 1970

ABSTRACT

A detailed analysis of the operation of the second harmonic magnetic modulator has been developed, with excitation voltage of either sinusoidal or rectangular form, and with the assumption of rectangular B-H loop of the cores in which the dynamic coercive force is taken into consideration. A simple expression for the second-harmonic component in the voltage waveform appearing across the output winding of the modulator has been derived.

As the coercive force is affected by the degree of saturation and by the frequency, the paper includes a discussion of the influence of the coercive force on both the amplitude and phase shift of the second harmonic output.

The comparison between the theoretical and experimental results has shown good agreement.

THE AUTHOR

Ibrahim M.H. Saad was born in Tanta, Egypt, on October 20, 1935. He received the B.Sc. degree in Electrical Engineering from the University of Alexandria, Egypt, in 1958 and the Ph.D. degree in Electrical Engineering from Moscow Power Institute, USSR in 1965. He was employed by Cairo Institute for Nuclear Research from 1958 to 1960. He is currently employed as a researcher in the Electrical Department of the National Institute of Standards, Cairo, Egypt. During 1969 he was on a Unesco Fellowship at the National Research Council of Canada. He is interested in nonlinear magnetic control devices, in general, with special attention to magnetic amplifier circuits.

CONTENTS

FIGURE CAPTIONS

Fig. 1 Circuit of the Modulator

Fig. 2 Rectangular Hysteresis Loop

Fig. 3 Ideal Magnetization Characterists

Fig. 4 Waveshapes for magnetic modulator with sinusoidal excitation (A) Supply Voltage, (B) Flux density without d.c. signal, (C) Flux density with d.c. signal, (D) Load current.

Fig. 5 Normalized amplitude of second harmonic current as function of nonconducting interval Θ

Fig. 6 Normalized amplitude of second harmonic current as function of normalized amplitude of sinusoidal excitation voltage.

Fig. 7 Phase angle of second harmonic current as function of normalized amplitude of sinusoidal excitation voltage

Fig. 8 Variation of second harmonic current amplitude with sinusoidal excitation voltage amplitude for the case: R_p=2.5KΩ, R_ℓ=5KΩ, R_c=500Ω, I_c=0.75 m.a.

Fig. 9 Variation of second harmonic current amplitude with sinusoidal excitation voltage amplitude for the case: R_p=3.2KΩ, R_ℓ=10KΩ, R_c=1KΩ, I_c=0.48 m.a.

Fig. 10 Variation of second harmonic current amplitude with sinusoidal excitation voltage amplitude for the case: R_p=5KΩ, R_ℓ=10KΩ, R_c=500Ω, I_c=0.75 m.a.

Fig. 11 Waveshapes for magnetic modulator with rectangular excitation. (A) Supply voltage, (B) Flux density without d.c. signal, (C) Flux density with d.c. signal, (D) Load current.

Fig. 12 Normalized amplitude of second harmonic current as function of normalized amplitude of rectangular excitation voltage.

Fig. 13 Phase angle of second harmonic current as function of normalized amplitude of rectangular excitation voltage.

Fig. 14 Variation of second harmonic current amplitude with rectangular excitation voltage amplitude for the case: R_p=5KΩ, R_ℓ=10KΩ, R_c=200Ω, I_c=1.12 m.a.

Fig. 15 Variation of second harmonic current amplitude with rectangular excitation voltage amplitude for the case: R_p=10KΩ, R_ℓ=10KΩ, R_c=200Ω, I_c=1.12m.a.

OPERATION OF THE SECOND-HARMONIC MAGNETIC MODULATOR WITH SINUSOIDAL AND SQUARE WAVE EXCITATION VOLTAGES

– I.M.H. Saad –

Introduction

The primary object of this paper is to develop an analytical expression for the second-harmonic component in the voltage waveform appearing across the output winding of the second-harmonic magnetic modulator of the type shown in Fig. 1. A review of literature indicates that very little work has been done concerning the analysis of the operation of this circuit. The expression for the second-harmonic component is derived for both sinusoidal and rectangular excitation voltages. In getting these expressions a method[1], which has been used in the analysis of magnetic amplifier circuits, is modified to suit this type of magnetic circuit .

The analysis of the modulator circuit is based on the assumption of a rectangular hysteresis loop of the core material as shown in Fig. 2. The hysteresis loops have vertical flanks and a width which is equal to double the dynamic coercive force H_c. The saturation branches of the hysteresis loops are horizontal. The values of H_c and B_s are determined from the major dynamic loops of the cores at the operating frequency. Previous analyses[2,3,4] have been based upon the idealized single valued B-H characteristic which neglects the hysteresis effect, as shown in Fig. 3. In one paper[3] the analysis has been simplified by representing the sinusoidal excitation current as a trapezoidal function of time. The assumption of the rectangular B-H loop is more realistic if we take into consideration the fact that the signal sensitivity of this type of modulator

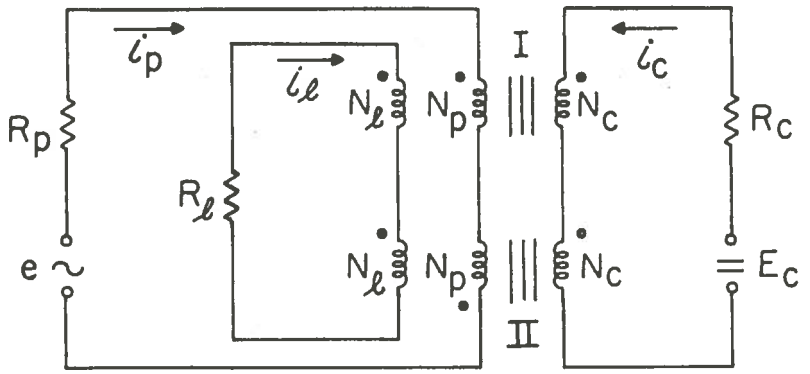

Fig. 1 Circuit of the modulator

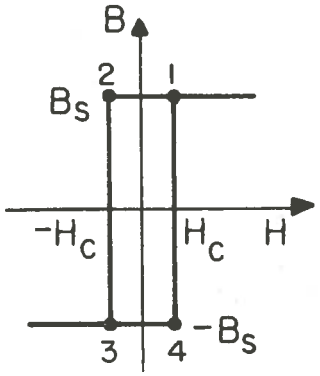

Fig. 2 Rectangular hysteresis loop

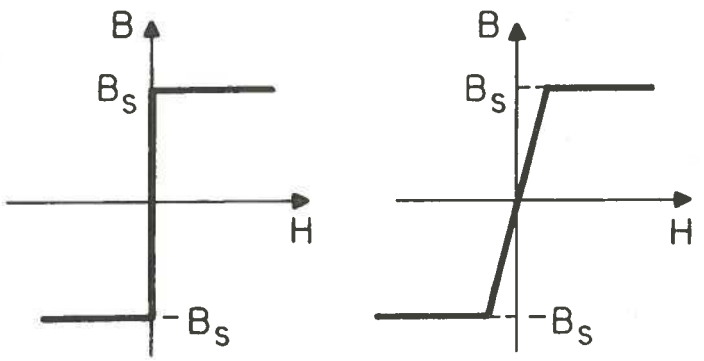

Fig. 3 Ideal magnetization characteristics

rises and the noise level falls with increasing excitation frequency[2].

The analysis is based on the assumption that in the absence of the d.c. signal the peak value of the excitation voltage is such that the cores are in the normal excitation or overexcitation condition, i.e. E_m or E_r has such a magnitude as to make the flux density excursion B_m or B_r equal to or greater than B_s.

The method of analysis developed in this work is described in the following steps:

1. With the use of the normalized quantities which are listed in the nomenclature the following set of nonlinear differential equations and the m.m.f. equations of the cores are formed. These equations are general equations which describe the behaviour of the circuit at any instant.

$$i'_c R'_c + A'\left(\frac{dB_I}{dt} + \frac{dB_{II}}{dt}\right) = E'_c \qquad (1)$$

$$i'_\ell R'_\ell + A'\left(\frac{dB_I}{dt} + \frac{dB_{II}}{dt}\right) = 0 \qquad (2)$$

$$i'_p R'_p + A'\left(\frac{dB_I}{dt} - \frac{dB_{II}}{dt}\right) = e' \qquad (3)$$

$$i'_p + i'_c + i'_\ell = \ell' H_I \qquad (4)$$

$$i'_c + i'_\ell - i'_p = \ell' H_{II} \qquad (5)$$

2. The analysis procedure of the magnetic modulator circuit is divided into

Case (a): when the d.c. input signal is equal to zero,

Case (b): when the d.c. signal is present.

3. Time intervals are found for cases a and b within half a period of the excitation voltage from the waveforms of the flux densities of the two cores. Within any time interval each core may have one of two conditions; saturated or unsaturated. Consequently the set of nonlinear differential equations 1 through 3 will become linear within the limits of any interval.

4. The expressions for the load current and the boundary angles of the time intervals for both cases a and b may be determined from the solution of the set of equations 1 through 5 for every interval.

5. The limiting angles of the intervals in the presence of the d.c. signal can be expressed in terms of the limiting angles of the intervals in the absence of the d.c. signal.

6. Taking step 4 into consideration an expression can be derived for the second-harmonic component of the load current by the use of Fourier's series expansion.

PART I. OPERATION WITH SINUSOIDAL WAVE EXCITATION VOLTAGE

Case a: Zero D.C. Signal (E_c=0)

The waveshapes of the excitation voltage and the flux densities

of the two cores are shown in Fig. 4(A) and (B). The flux density waves of the two cores are symmetrical in the absence of the d.c. signal. Within half a period of the excitation voltage two intervals can be found. These intervals depend on the condition of the cores; saturated or unsaturated.

Nonconduction Interval

This interval continues from $\omega t = \alpha$ to $\omega t = \beta$. The two cores in this interval are unsaturated. The observation of the flux density waves and the B-H loop gives the following relations:

$$H_I = H_c$$

$$H_{II} = -H_c$$

$$\frac{dB_{II}}{dt} = -\frac{dB_I}{dt}$$

Taking these relations into consideration the following equations may be obtained from equations 1 through 5:

$$i_c' = i_\ell' = 0$$

$$i_p' = \ell' H_c \tag{6}$$

$$\frac{dB_I}{dt} = \frac{1}{2A'}\left(E_m' \sin \omega t - \ell' R_p' H_c\right) \tag{7}$$

Conduction Interval

The limits of this interval are $\omega t = \beta$ and $\omega t = \pi + \alpha$

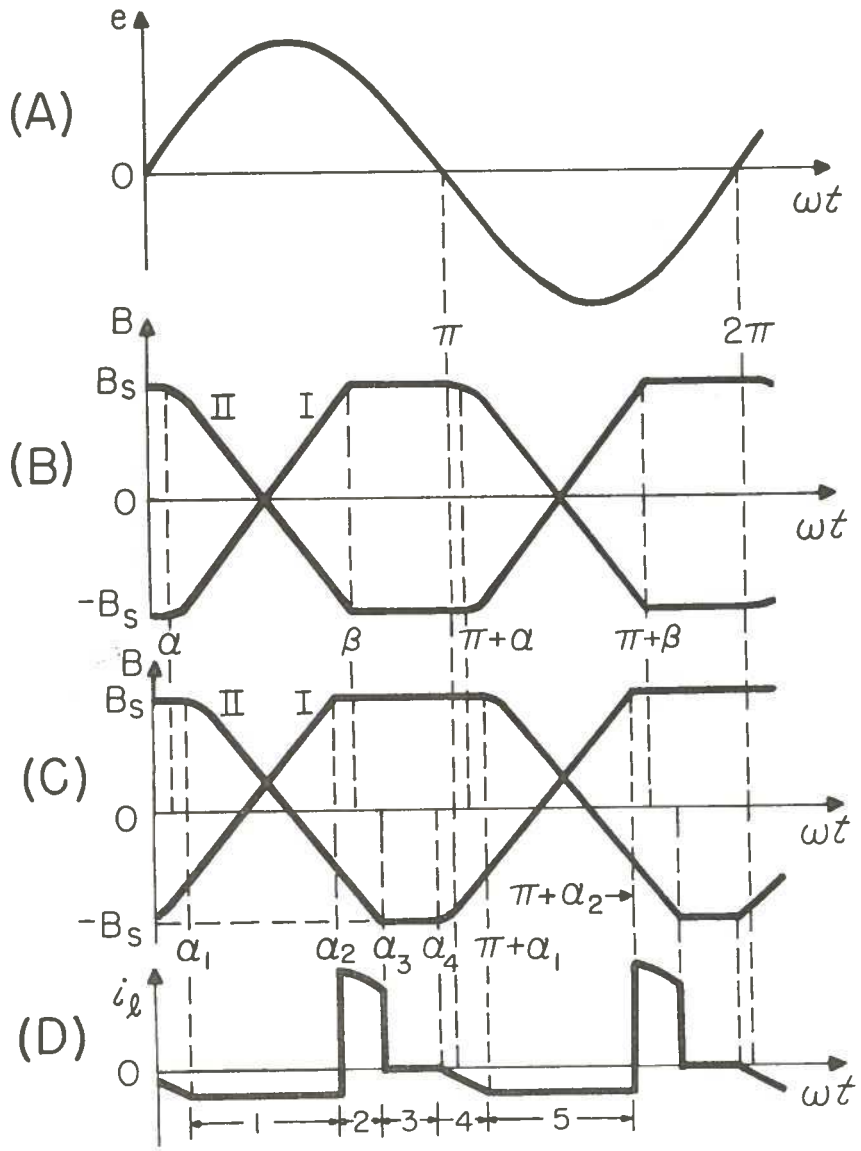

Fig. 4 Waveshapes for magnetic modulator with sinusoidal excitation. (A) Supply voltage, (B) Flux density without d.c. signal, (C) Flux density with d.c. signal, (D) Load current.

and both cores are saturated, therefore:

$$\frac{dB_I}{dt} = \frac{dB_{II}}{dt} = 0$$

The substitution of this condition into equations 1, 2 and 3 gives

$$i'_c = i'_\ell = 0$$

$$i'_p = \frac{E'_m}{R'_p} \sin \omega t \tag{8}$$

The boundary angles α and β may be obtained from two conditions:

1. At the end of the conduction interval the current i'_p must be equal to $-\ell' H_c$. Consequently, substituting $\omega t = \pi + \alpha$ in equation 8 yields:

$$\sin \alpha = \frac{\ell' R'_p H_c}{E'_m} \tag{9}$$

2. Integrating equation 7 between the limits $\omega t = \alpha$ and $\omega t = \beta$ and substituting the boundary conditions for the flux density in core I, namely, $B_I = -B_s$ at $\omega t = \alpha$ and $B_I = B_s$ at $\omega t = \beta$, then

$$\cos \alpha - \cos \beta - \frac{\ell' R'_p H_c}{E'_m} (\beta - \alpha) = \frac{4A' \omega B_s}{E'_m} \tag{10}$$

The substitution of $H_c = 0$ in equation 9 gives $\alpha = 0$, therefore equation 10 reduces to

$$1 - \cos \beta = \frac{4A' \omega B_s}{E'_m} \tag{11}$$

which determines the value of the conduction angle β for the case of the idealized B-H characteristic of Fig. 3.

Case b: The D.C. signal is present.

The presence of the small d.c. signal upsets the symmetry of the flux density waves and creates new intervals within half a period of the excitation voltage, as shown in Fig. 4(C). The width of these intervals depends on the value of the d.c. ampere-turns. According to Fig. 4(C) four intervals can be found within half a cycle. The limiting angles of these intervals and the condition of the cores are listed in the following table:

No. of Interval	Limits of Interval	Conditions of the Cores	
		Core I	Core II
1	α_1 and α_2	unsaturated	unsaturated
2	α_2 and α_3	saturated	unsaturated
3	α_3 and α_4	saturated	saturated
4	α_4 and $\pi + \alpha_1$	saturated	unsaturated

The equations which describe the behaviour of the circuit during each interval may be derived from the set of equations 1 through 5. Two conditions must be taken into account:

1. For any core in the unsaturated condition $H = \pm H_c$, where the sign + or - applies, depending on whether the flux density excursion is ascending from $-B_s$ to B_s or descending from B_s to $-B_s$.

2. $\frac{dB}{dt}$ is equal to zero for any core in the saturated condition.

Interval 1

The m.m.f. equations for this interval are

$$\left.\begin{aligned} \ell' H_c &= i'_p + i'_c + i'_\ell \\ -\ell' H_c &= i'_c + i'_\ell - i'_p \end{aligned}\right\} \tag{12}$$

These two equations show that the sum i'_p plus $(i'_c + i'_\ell)$ and the difference i'_p minus $(i'_c + i'_\ell)$ are equal to the same value $\ell' H_c$. Therefore the following two relations must be valid:

$$i'_c = -i'_\ell \tag{13}$$

$$i'_p = \ell' H_c \tag{14}$$

Consequently, the following relations can be deduced from equations 1, 2, 3, 13 and 14:

$$i'_\ell = \frac{-E'_c}{R'_c + R'_\ell} \tag{15}$$

$$\frac{dB_I}{dt} = \frac{1}{2A'} \left[E'_m \sin \omega t + \frac{R'_\ell}{R'_c + R'_\ell} E'_c - \ell' R'_p H_c \right] \tag{16}$$

$$\frac{dB_{II}}{dt} = \frac{1}{2A'} \left[-E'_m \sin \omega t + \frac{R'_\ell}{R'_c + R'_\ell} E'_c + \ell' R'_p H_c \right] \tag{17}$$

Interval 2

The m.m.f. equation of core II becomes

$$i'_c + i'_\ell - i'_p = - \ell' H_c \tag{18}$$

and the expressions for the currents in the modulator circuits and the flux density derivative for core II are found from equations 1, 2, 3 and 18.

$$i'_\ell = \frac{R'_c}{a} \left[E'_m \sin \omega t - \ell' R'_p H_c - \frac{R'_p}{R'_c} E'_c \right] \tag{19}$$

$$i'_c = \frac{R'_\ell}{a} \left[E'_m \sin \omega t - \ell' R'_p H_c + \left(\frac{R'_p}{R'_\ell} + 1 \right) E'_c \right] \tag{20}$$

$$i'_p = \frac{R'_\ell}{a} \left[\left(1 + \frac{R'_c}{R'_\ell} \right) E'_m \sin \omega t + \ell' R'_c H_c + E'_c \right] \tag{21}$$

$$\frac{dB_{II}}{dt} = \frac{-R'_\ell R'_c}{a\, A'} \left(E'_m \sin \omega t - \ell' R'_p H_c - \frac{R'_p}{R'_c} E'_c \right) \tag{22}$$

where $a = R'_p (R'_\ell + R'_c) + R'_\ell R'_c$

Interval 3

During this interval, the circuit equations are

$$i'_\ell = 0 \tag{23}$$

$$i'_c = \frac{E'_c}{R'_c} \tag{24}$$

$$i'_p = \frac{E'_m}{R'_p} \sin \omega t \tag{25}$$

Interval 4

The m.m.f. equation of core II is

$$i'_c + i'_\ell - i'_p = \ell' H_c \tag{26}$$

and the current and flux density equations are

$$i'_\ell = \frac{R'_c}{a}\left[E'_m \sin \omega t + \ell' R'_p H_c - \frac{R'_p}{R'_c} E'_c\right] \tag{27}$$

$$i'_c = \frac{R'_\ell}{a}\left[E'_m \sin \omega t + \ell' R'_p H_c + \left(\frac{R'_p}{R'_\ell} + 1\right) E'_c\right] \tag{28}$$

$$i'_p = \frac{R'_\ell}{a}\left[\left(\frac{R'_c}{R'_\ell} + 1\right) E'_m \sin \omega t - \ell' R'_c H_c + E'_c\right] \tag{29}$$

$$\frac{dB_{II}}{dt} = \frac{-R'_\ell R'_c}{a\ A'}\left[E'_m \sin \omega t + \ell' R'_p H_c - \frac{R'_p}{R'_c} E'_c\right] \tag{30}$$

Interval 5

The rate of change of flux density for core II during this interval is:

$$\frac{dB_{II}}{dt} = \frac{1}{2A'}\left[\frac{R'_\ell}{(R'_c + R'_\ell)} E'_c - E'_m \sin \omega t - \ell' R'_p H_c\right] \tag{31}$$

Four relationships which determine the values of the angles α_1, α_2, α_3 and α_4 may be found from the following conditions:

(a) At the end of interval 4, which corresponds to point 2 on the B-H loop, core I comes out of positive saturation. Hence the sum of the m.m.f.'s at that point is equal to $-\ell' H_c$. Taking

this condition into consideration and substituting $\omega t = \pi + \alpha_1$ in equations 27 through 29 an expression for α_1 can be deduced in the form

$$\sin \alpha_1 = \frac{R'_p \ell' H_c}{E'_m} + \frac{R'_\ell}{(R'_c + R'_\ell)} \frac{E'_c}{E'_m} \tag{32}$$

(b) At the end of interval 3, which corresponds to point 4 on the B-H loop, core II comes out of negative saturation. Therefore the difference of the m.m.f.'s $(i'_c + i'_\ell)$ minus i'_p is equal to $\ell' H_c$. Utilizing this condition and equations 23 through 25 yields:

$$\sin \alpha_4 = \frac{R'_p}{R'_c} \frac{E'_c}{E'_m} - \frac{R'_p \ell' H_c}{E'_m} \tag{33}$$

(c) At the beginning of the first and the end of the fifth intervals the flux density in core II has the same value B_s. Consequently the following relationship is valid:

$$\int_{\alpha_1}^{(\pi + \alpha_2)} \frac{dB_{II}}{dt} \, d\omega t = 0 \tag{34}$$

Substituting equations 17, 22, 30 and 31 into the preceding equation and integrating yields:

$$\cos\alpha_1 + \cos\alpha_2 + \cos\alpha_4 - \cos\alpha_3 = \frac{ab_1}{R'_c R'_\ell} (\alpha_2 - \alpha_1) + (b_2 + b_3)(\alpha_3 - \alpha_2) +$$

$$(b_2 - b_3)(\pi + \alpha_1 - \alpha_4) \tag{35}$$

where $b_1 = \frac{R'_\ell}{R'_c + R'_\ell} \frac{E'_c}{E'_m}$, $b_2 = \frac{R'_p}{R'_c} \frac{E'_c}{E'_m}$, $b_3 = \frac{\ell' R'_p H_c}{E'_m}$.

(d) The flux density excursion in core II from positive saturation at $\omega t = \alpha_1$ to negative saturation at $\omega t = \alpha_3$ is equal to $-2B_s$. Therefore the integration of the rate of change of the flux density between these limits is equal to $-2B_s$, namely

$$\int_{\alpha_1/\omega}^{\alpha_2/\omega} \frac{dB_{II}}{dt}\, dt + \int_{\alpha_2/\omega}^{\alpha_3/\omega} \frac{dB_{II}}{dt}\, dt = -2B_s \qquad (36)$$

The evaluation of this integral after the substitution of equations 17 and 22 into it gives

$$\frac{-4A'\omega B_s}{E'_m} = \frac{2R'_\ell R'_c}{a} \left[\cos\alpha_3 - \cos\alpha_2 + (b_3+b_2)(\alpha_3-\alpha_2)\right] + \cos\alpha_2 - \cos\alpha_1$$

$$+ (b_1+b_3)(\alpha_2-\alpha_1) \qquad (37)$$

A realistic and valuable approach is discussed in the following for the evaluation of the angles α_1, α_2, α_3 and α_4 from equations 32, 33, 35 and 37. This approach is based on the assumption of a low-level d.c. signal. Careful observation of the flux density wave forms in the absence and presence of the d.c. signal shows that the presence of the d.c. signal is equivalent to the following effects on the flux density waveform:

1. The conduction angle β is advanced by a certain

amount $\Delta\alpha_2$ for core I and retarded by another amount $\Delta\alpha_3$ for core II.

2. The limiting angle $\pi + \alpha$ is retarded by an amount $\Delta\alpha_1$ for core I and advanced by another amount $\Delta\alpha_4$ for core II. Under these conditions the boundary angles of the intervals can be expressed as

$$\alpha_1 = \alpha + \Delta\alpha_1 \tag{38}$$

$$\alpha_2 = \beta - \Delta\alpha_2 \tag{39}$$

$$\alpha_3 = \beta + \Delta\alpha_3 \tag{40}$$

$$\alpha_4 = \pi + \alpha - \Delta\alpha_4 \tag{41}$$

and the values of $\Delta\alpha_1$, $\Delta\alpha_2$, $\Delta\alpha_3$ and $\Delta\alpha_4$ are determined from the following equations:

$$\Delta\alpha_1 = \frac{R'_\ell}{(R'_c + R'_\ell)} \frac{E'_c}{E'_m} \frac{1}{\cos\ \alpha} \tag{42}$$

$$\Delta\alpha_4 = \frac{R'_p}{R'_c} \frac{E'_c}{E'_m} \frac{1}{\cos\ \alpha} \tag{43}$$

$$\Delta\alpha_2 = \frac{(\beta - \alpha)\ \cos\ \alpha}{(\sin\ \beta - \sin\ \alpha)}\ \Delta\alpha_1 \tag{44}$$

$$\Delta\alpha_3 = \frac{(\beta - \alpha)\ \cos\ \alpha}{(\sin\ \beta - \sin\ \alpha)}\ \Delta\alpha_4 \tag{45}$$

The derivation of these expressions from equations 32, 33, 35

and 37 is given in Appendix I.

The instantaneous value of the second harmonic component of the load current may be defined in the form

$$i_2 = I_{2a} \sin (2\omega t + \phi_2) \tag{46}$$

or in the normalized form

$$i'_2 = I'_{2a} \sin (2\omega t + \phi_2) \tag{47}$$

where $i'_2 = N_\ell \, i_2$, $I'_{2a} = N_\ell \, I_{2a}$

In Appendix II is given the derivation of the following expressions for the amplitude and phase shift of the second harmonic component. This derivation is based on the use of Fourier series expansion and equations of the load current during intervals 1, 2, 3 and 4.

$$I'_{2a} = \frac{2}{\pi} \frac{E'_c}{(R'_c + R'_\ell)} \left[\frac{1}{2} (1 - \cos 2\theta) + \theta^2 - \theta \sin 2\theta\right]^{\frac{1}{2}} \tag{48}$$

$$\phi_2 = \tan^{-1} \left[\frac{\sin 2\alpha - \sin 2\beta + 2\theta \cos 2\beta}{\cos 2\beta - \cos 2\alpha + 2\theta \sin 2\beta}\right] \tag{49}$$

where

$$\theta = \beta - \alpha \tag{50}$$

Equation 48 can be rewritten in the form

$$I_{2a} = \frac{2}{\pi} \frac{E_c}{\frac{N_c}{N_\ell}\left[\left(\frac{N_\ell}{N_c}\right)^2 R_c + R_\ell\right]} \left[\frac{1}{2} (1 - \cos 2\theta) + \theta^2 - \theta \sin 2\theta\right]^{\frac{1}{2}} \tag{51}$$

DISCUSSION OF THE THEORETICAL RESULTS

1. The amplitude and phase shift of the second harmonic component of the load current can be determined easily from equations 49 and 51. The values of the angles α and β are found from equations 9 and 10 for a given excitation amplitude and frequency.

2. Equation 51 shows that the amplitude of the second harmonic current is linearly related to the input d.c. signal and changes in phase by 180 degrees according to the actual polarity of the d.c. signal.

3. Defining

$$\frac{2}{\pi} \frac{E_c}{\frac{N_c}{N_\ell}\left[\left(\frac{N_\ell}{N_c}\right)^2 R_c + R_\ell\right]} = I_{2m} \tag{52}$$

equation 51 transforms into

$$\frac{I_{2a}}{I_{2m}} = \left[\frac{1}{2}(1 - \cos 2\theta) + \theta^2 - \theta \sin 2\theta\right]^{\frac{1}{2}} \tag{53}$$

In Fig. 5 the normalized quantity I_{2a}/I_{2m} is plotted against the value of the non-conduction interval θ. This figure shows that the amplitude of the second harmonic component depends on the width of the non-conduction interval and its value changes non-linearly from a maximum at $\theta = 180°$ to zero at $\theta = 0$.

It must be noted that in practical modulator circuits the maximum value of the second harmonic component does not occur

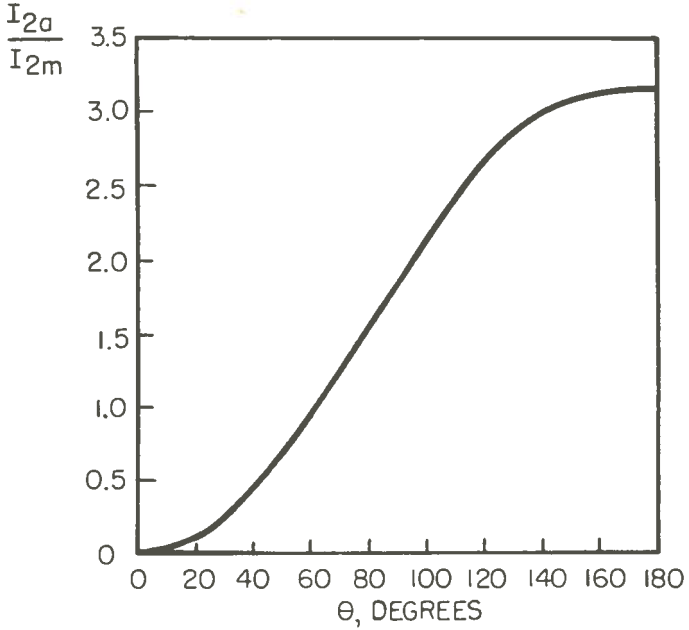

Fig. 5 Normalized amplitude of second harmonic current as function of nonconducting interval θ.

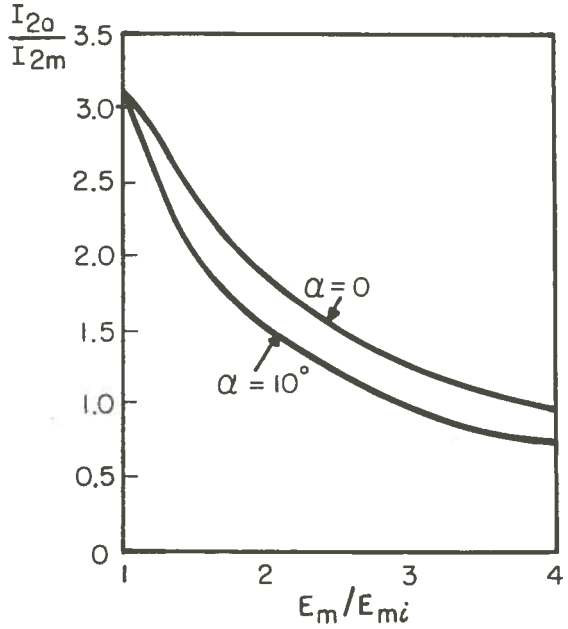

Fig. 6 Normalized amplitude of second harmonic current as function of normalized amplitude of sinusoidal excitation voltage.

since the value of the non-conduction interval is permanently less than 180°. This is due to the influence of the coercive force on the loss angle α.

4. For the ideal case when H_c is equal to zero the non-conduction interval will be equal to the conducting angle β and equation 10 transforms into

$$1 - \cos \beta = \frac{4A' \omega B_s}{E'_m} \tag{54}$$

The theoretical value of the excitation voltage amplitude, which corresponds to the maximum value of the second harmonic amplitude may be found by substituting β = 180° in equation 54

$$E'_{mi} = 2A' \omega B_s \tag{55}$$

Accordingly equation 10 may be written in terms of E'_{mi} as follows:

$$\cos \alpha - \cos \beta - (\beta - \alpha) \sin \alpha = 2 \frac{E'_{mi}}{E'_m} \tag{56}$$

On the basis of equation 50, 53 and 56 a normalized plot of I_{2a}/I_{2m} against E_m/E_{mi} is represented in Fig. 6 for two values of the loss angle. These curves show the manner in which the amplitude of the second harmonic current is affected by the value of the amplitude of the excitation voltage and the coercive force.

5. The variation in the phase angle of the second harmonic output current due to different values of E_m/E_{mi} is plotted in

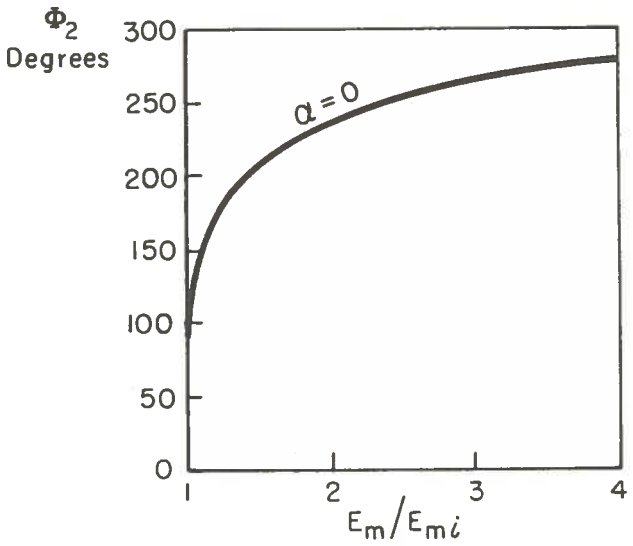

Fig. 7 Phase angle of second harmonic current as function of normalized amplitude of sinusoidal excitation voltage.

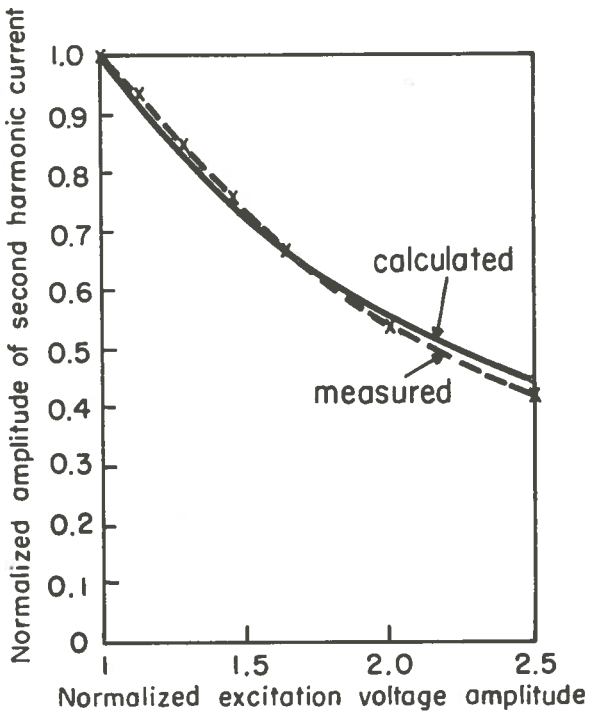

Fig. 8 Variation of second harmonic current amplitude with sinusoidal excitation voltage amplitude for the case: $R_p = 2.5\,K\Omega$, $R_\ell = 5\,K\Omega$, $R_c = 500\,\Omega$, $I_c = 0.75$ m.a.

Fig. 7 for $\alpha = 0$. This plot is derived from equations 49 and 56. The analysis of these equations indicates that for practical values of the coercive force the change in the phase of I_{2a}/I_{2m} from that given in Fig. 7 is negligible.

COMPARISON BETWEEN THEORETICAL AND PRACTICAL MEASUREMENTS

The toroidal cores were made from Hymu "80", .002 inch tape thickness in aluminum case. The cores have the following dimensions: inside diameter 2.5 inch, outside diameter 3 inch, height 0.5 inch. The net cross-sectional area of flux path = 0.1063 inch square and the mean path length = 8.639 inch. The number of turns of the windings on each core were N_p = 1000 turns, N_c = 200 turns and N_ℓ = 2000 turns. The frequency of the excitation voltage was 400 c/s.

From the major dynamic B-H loop of the cores the values of the dynamic coercive force and the saturation flux density were found to be:

$$H_c = 0.12 \text{ oersted}$$

$$B_s = 7500 \text{ gauss.}$$

At a fixed value of the d.c. signal the amplitude of the second harmonic output voltage was measured on a wave analyzer for different values of the excitation voltage amplitude. The results of the measurements can be normalized with respect to the values corresponding to the normal excitation condition. This is done for three sets of values of the parameters of the

circuit and the experimental curves are compared with the theoretical behaviour described by equations 9, 10, 50 and 51 in Figs. 8, 9 and 10. In Fig. 8, where R_p = 2.5 K ohms, the effect of the loss angle on the calculated results is negligible and the theoretical curve was plotted for the ideal case $\alpha = 0$.

There are several sources of error which affect both the calculated and measured results, mainly:

1. The difficulties in measuring the magnetic parameters of the cores.

2. The deviation of the actual shape of the B-H loop from the rectangular characteristic.

3. The asymmetry and noise which may exist in the waveform of the a.c. excitation source especially at higher values of the excitation amplitude. If allowance is made for the preceding sources of error, the theoretical results are in good agreement with the experimental ones.

PART II. OPERATION WITH RECTANGULAR WAVE EXCITATION VOLTAGE

Case a. Zero D.C. Signal ($E_c = 0$)

For this case two intervals can be found in Fig. 11(A) and (B) within half a cycle of the excitation voltage; the non-conduction interval from 0 to β and the conduction interval from β to π. The value of β can be determined from the following equation:

$$\beta = \frac{4A' \omega B_s}{E'_r - \ell' R'_p H_c} \tag{57}$$

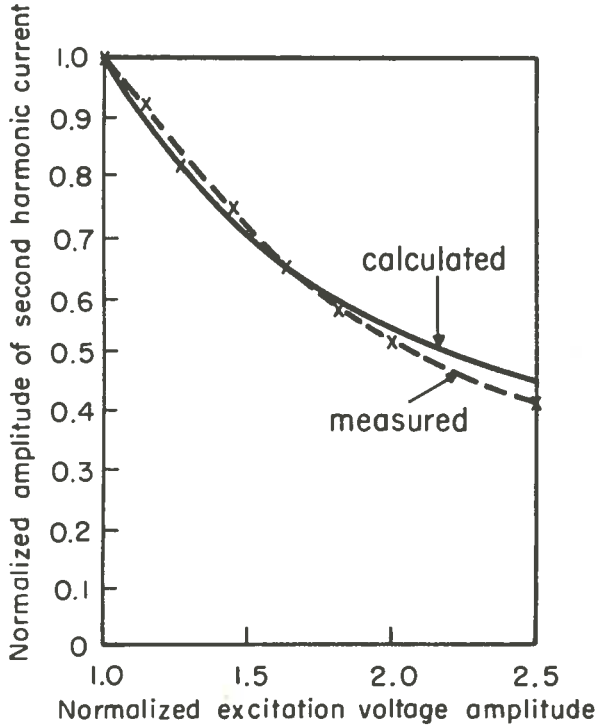

Fig. 9 Variation of second harmonic current amplitude with sinusoidal excitation voltage amplitude for the case: $R_p = 3.2\,K\Omega$, $R_\ell = 10K\Omega$, $R_c = 1K\Omega$, $I_c = 0.48$ m.a.

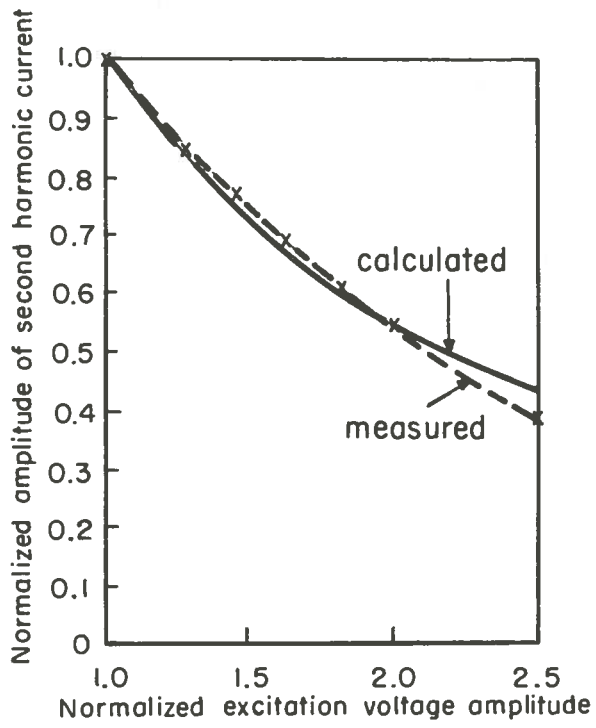

Fig. 10 Variation of second harmonic current amplitude with sinusoidal excitation voltage amplitude for the case: $R_p = 5K\Omega$, $R_\ell = 10K\Omega$, $R_c = 500\Omega$, $I_c = 0.75$ m.a.

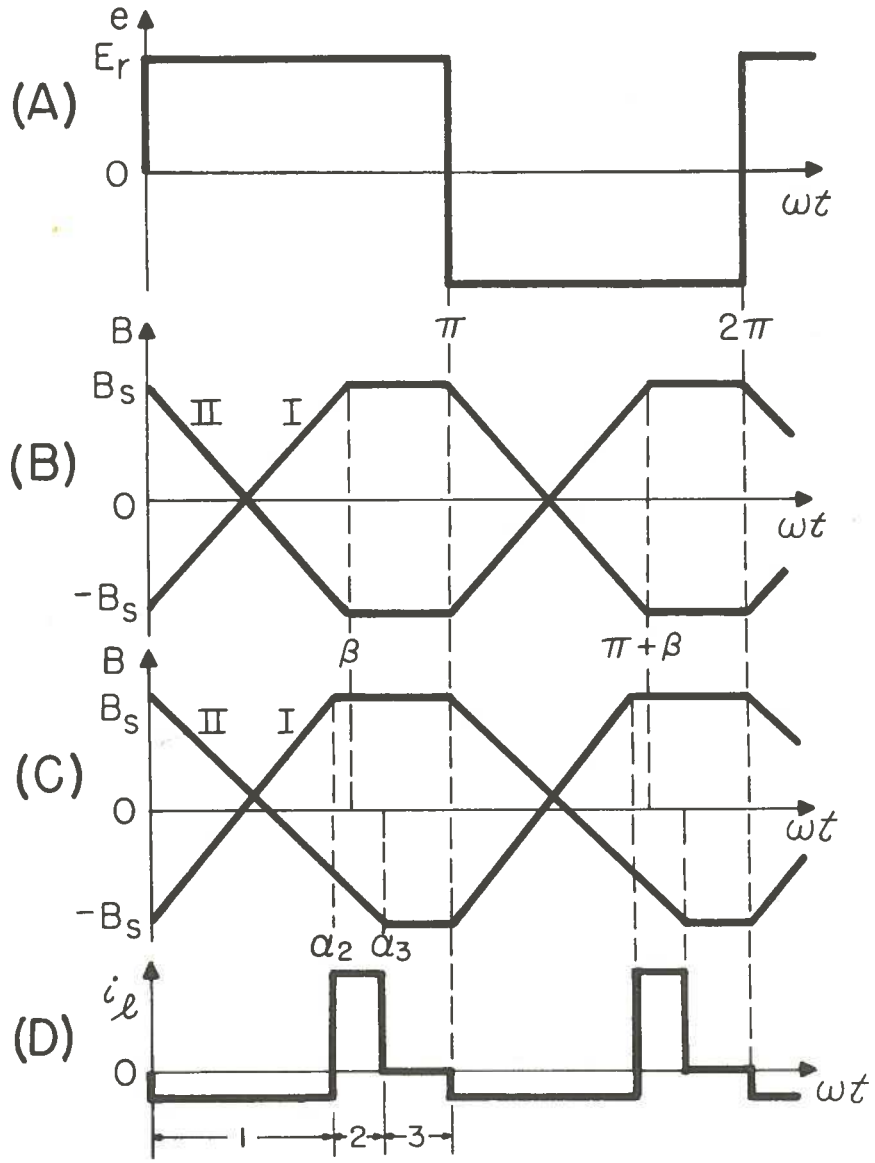

Fig. 11 Waveshapes for magnetic modulator with rectangular excitation. (A) Supply voltage, (B) Flux density without d.c. signal, (C) Flux density with d.c. signal, (D) Load current.

The derivation of this equation from the basic equations 1 through 5 is given in Appendix III. It must be noted that this expression is valid only for the conditions of normal and over-excitation, i.e. when the value of β is equal to or less than π.

Case b. The D.C. Signal is Present

Figs. 11(C) and (D) show the instantaneous values of the flux densities in the cores I and II and also the current in the load circuit for this case. The effect of the d.c. signal on the flux density waveform is to advance the conduction angle β by an amount $\Delta\alpha_2$ for core I and retard it by another amount $\Delta\alpha_3$ for core II. Accordingly three intervals can be found within half a cycle of the excitation voltage. The magnetic conditions of the cores within every interval are listed in the following table:

No. of Interval	Limits of Interval	Condition of the Cores	
		Core I	Core II
1	0 and α_2	unsaturated	unsaturated
2	α_2 and α_3	saturated	unsaturated
3	α_3 and π	saturated	saturated

Taking this table into consideration all equations for intervals 1, 2 and 3 of Part I apply also to the same intervals of Part II. The only modification is the substitution of the quantity E_r for $E_m \sin \omega t$ in all the given equations.

Two equations are required for the evaluation of the

boundary angles α_2 and α_3. These equations can be obtained by making use of the conditions c and d in Part I and modifying equations 34 and 36 into:

$$\int_{o}^{\pi + \alpha_2} \frac{dB_{II}}{dt}\, d\omega t = 0 \tag{58}$$

$$\int_{o}^{\alpha_2/\omega} \frac{dB_{II}}{dt}\, dt + \int_{\alpha_2/\omega}^{\alpha_3/\omega} \frac{dB_{II}}{dt}\, dt = -2B_s \tag{59}$$

Substituting the expressions of $\frac{dB_{II}}{dt}$ for the different intervals and integrating equations 58 and 59 yields:

$$b'_1\, \alpha_2 - \frac{R'_\ell\, R'_c}{a} (1 - b'_3 - b'_2)(\alpha_3 - \alpha_2) = 0 \tag{60}$$

$$\frac{4\omega\, A'B_s}{E'_r} = 2\, \frac{R'_\ell R'_c}{a} (1 - b'_3 - b'_2)(\alpha_3 - \alpha_2) + (1 - b'_3 - b'_1)\, \alpha_2 \tag{61}$$

where $b'_1 = \frac{R'_\ell}{(R'_c + R'_\ell)} \frac{E'_c}{E'_r}$, $b'_2 = \frac{R'_p}{R'_c} \frac{E'_c}{E'_r}$, $b'_3 = \frac{\ell' R'_p H_c}{E'_r}$.

The same approach which has been used for the determination of the boundary angles of the intervals in the case of sinusoidal excitation can be extended to cover the case of rectangular excitation. Defining

$$\left.\begin{aligned} \alpha_2 &= \beta - \Delta\alpha_2 \\ \alpha_3 &= \beta + \Delta\alpha_3 \end{aligned}\right\} \tag{62}$$

and utilizing these expressions the solution of equations 60 and 61 yields

$$\Delta\alpha_2 = \beta - \frac{\dfrac{4A'\ \omega B_s}{E'_r}}{1 - \dfrac{\ell' R'_p H_c}{E'_r} + \dfrac{R'_\ell}{(R'_c + R'_\ell)} \dfrac{E'_c}{E'_r}} \tag{63}$$

$$\Delta\alpha_3 = \frac{\dfrac{4A'\ \omega B_s}{E'_r}}{1 - \dfrac{\ell' R'_p H_c}{E'_r} - \dfrac{R'_p}{R'_c} \dfrac{E'_c}{E'_r}} - \beta \tag{64}$$

The instantaneous value of the load current during the half period from 0 to π can be determined from equations 15, 19 and 23 after the substitution of E_r for $E_m \sin \omega t$

$$\begin{aligned} i'_\ell &= \frac{-E'_c}{(R'_c + R'_\ell)} && \alpha_2 \geq \omega t \geq 0 \\ &= \frac{R'_c}{a}\left(E'_r - \ell' R'_p H_c - \frac{R'_p}{R'_c} E'_c \right) && \alpha_3 \geq \omega t \geq \alpha_2 \\ &= 0 && \pi \geq \omega t \geq \alpha_3 \end{aligned} \tag{65}$$

The coefficients of the Fourier series for the second harmonic component of the load current are obtained from the preceding equation by the same procedure of Appendix I in the following form:

$$A_o = 0 \tag{66}$$

$$A_1 = \frac{E'_c}{\pi(R'_c + R'_\ell)} (2\beta \cos 2\beta - \sin 2\beta) \tag{67}$$

$$B_1 = \frac{E'_c}{\pi(R'_c + R'_\ell)} (\cos 2\beta + 2\beta \sin 2\beta - 1) \tag{68}$$

These expressions were derived by the aid of equations 62 through 64.

The second harmonic component of the load current is expressed by the same equations 46 and 47 and its amplitude and phase shift are found from equations 67 and 68 in the form

$$I'_{2a} = \frac{2E'_c}{\pi(R'_c + R'_\ell)} \left[\frac{1}{2} (1 - \cos 2\beta) + \beta^2 - \beta \sin 2\beta\right]^{\frac{1}{2}} \tag{69}$$

$$\phi_2 = \tan^{-1} \left[\frac{2\beta \cos 2\beta - \sin 2\beta}{\cos 2\beta + 2\beta \sin 2\beta - 1}\right] \tag{70}$$

Substituting the normalized quantities from the nomenclature into equation 69 yields

$$I_{2a} = \frac{2}{\pi} \frac{E_c}{\frac{N_c}{N_\ell}\left[\left(\frac{N_\ell}{N_c}\right)^2 R_c + R_\ell\right]} \left[\frac{1}{2} (1 - \cos 2\beta) + \beta^2 - \beta \sin 2\beta\right]^{\frac{1}{2}} \tag{71}$$

Equations 70 and 71 express the phase shift and amplitude in terms of the d.c. input voltage, the parameters of both the input and load circuits and the conduction angle β, which is

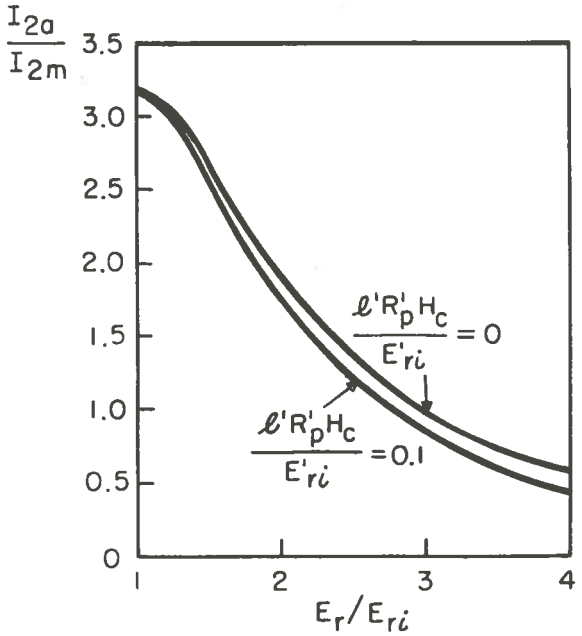

Fig. 12 Normalized amplitude of second harmonic current as function of normalized amplitude of rectangular excitation voltage.

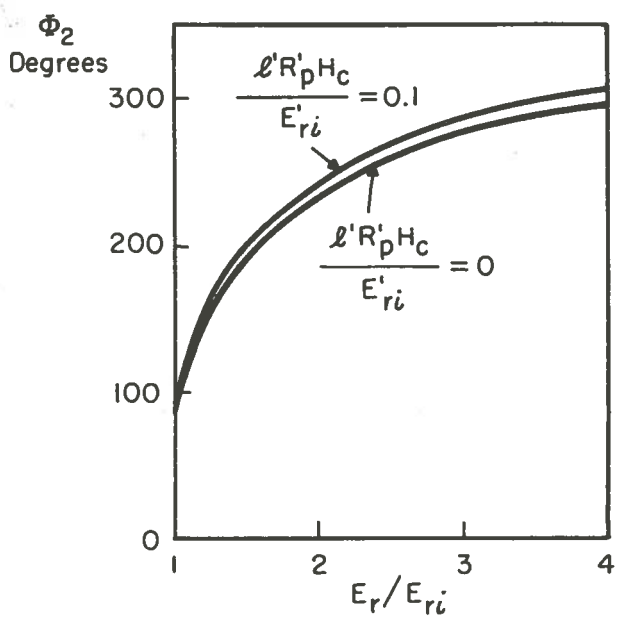

Fig. 13 Phase angle of second harmonic current as function of normalized amplitude of rectangular excitation voltage.

given by equation 57.

DISCUSSION OF THEORETICAL AND EXPERIMENTAL RESULTS

1. The observations of equations 48, 49 and 69, 70 indicates that the substitution of $\alpha = 0$ in the expressions of I'_{2a} and ϕ_2 for the case of sinusoidal excitation yields the same expressions which are derived for rectangular excitation. The coercive force in the case of rectangular excitation affects only the value of the conduction angle (equation 57) and the non-conduction interval will be larger than that for sinusoidal excitation. An important conclusion from these considerations is that the choice of rectangular excitation in practical problems is more valuable than sinusoidal excitation from the view point of the stability of the second harmonic output and the choice of higher excitation frequency.

2. The normalized plot of Fig. 5 is also valid for the case of rectangular excitation after the substitution of β for θ in that figure.

3. Consider the ideal case when H_c is equal to zero, then equation 57 transforms into

$$\beta = \frac{4A'\omega B_s}{E'_r} \tag{72}$$

The excitation amplitude for the ideal condition of normal excitation can be found from the preceding equation by substituting $\beta = \pi$

$$E'_{ri} = \frac{4}{\pi} A' \omega B_s \tag{73}$$

Accordingly equation 57 can be written in the form

$$\beta = \frac{\pi}{\frac{E'_r}{E'_{ri}} - \frac{\ell' R'_p H_c}{E'_{ri}}} \tag{74}$$

On the basis of equations 70, 71 and 74 the effect of variation of amplitude of the rectangular excitation voltage on both amplitude and phase shift of the second harmonic current is plotted in Figs. 12 and 13 for the ideal case when H_c is equal to zero. To show the influence of the coercive force on both I_{2a} and ϕ_2 other curves are plotted in the same figures for the case when $\ell' R'_p H_c / E'_{ri} = 0.1$. This value is chosen to correspond with practical parameters of the modulator circuit.

4. The same experimental circuit and method of measurement of Part I were used in the case of rectangular excitation. The frequency of excitation was also 400 c/s and the value of H_c was found to be 0.1 oersted. The comparison between the experimental and theoretical results is given in Figs. 14 and 15 for two sets of values of the parameters of the circuit. Causes of the noticeable discrepancy between the measured and theoretical curves at high values of R_p (Fig. 15) are believed to be the following:

(a) At lower values of excitation voltage the value of R_p becomes comparable to the value of the actual differential reactance around the knee of the normal induction curve.

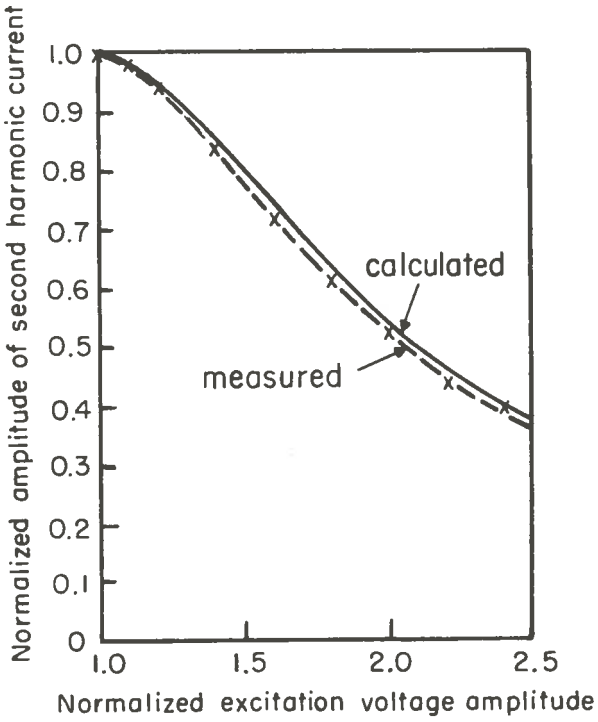

Fig. 14 Variation of second harmonic current amplitude with rectangular excitation voltage amplitude for the case: $R_p = 5\ K\Omega$, $R_\ell = 10K\Omega$, $R_c = 200\Omega$, $I_c = 1.12$ m.a.

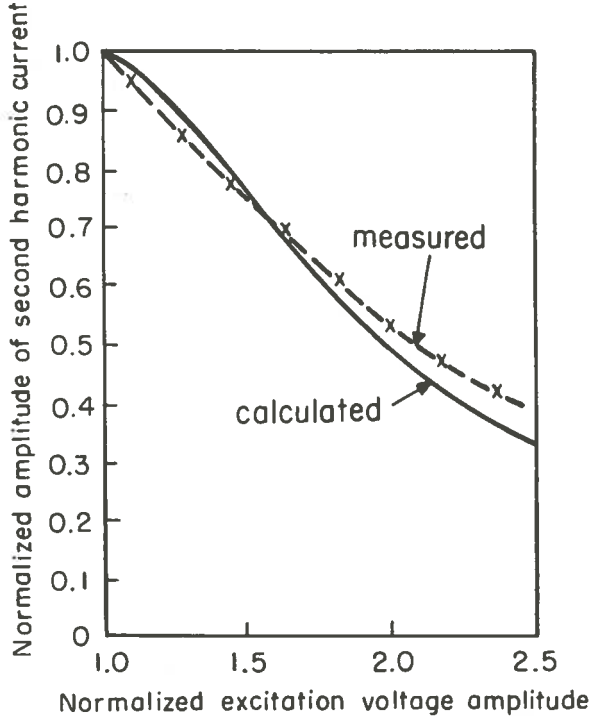

Fig. 15 Variation of second harmonic current amplitude with rectangular excitation voltage amplitude for the case: $R_p = 10K\Omega$, $R_\ell = 10K\Omega$, $R_c = 200\Omega$, $I_c = 1.12$ m.a.

(b) The excitation waveform is distorted at higher values of excitation voltage.

Conclusion

The second harmonic magnetic modulator has been analysed, with the excitation voltage of either sinusoidal or rectangular form, and with the assumption that the cores have a rectangular hysteresis loop in which the dynamic coercive force is taken into consideration.

An expression which determines the steady state amplitude and phase of the second harmonic component of the load current has been derived for both sinusoidal and rectangular excitations. This expression is sufficiently simple and accurate for engineering purposes. The close agreement between the theoretical and experimental results supports the validity of the developed theory.

The analysis indicates that the choice of rectangular excitation voltage improves the stability of the second harmonic output and gives higher limit to the choice of excitation frequency.

Acknowledgment

The author wishes to thank N.L. Kusters, M.P. MacMartin and W.J.M. Moore for many helpful discussions.

The work described was carried out at the National Research Council of Canada.

APPENDIX I

For small values of $\Delta\alpha_1$, $\Delta\alpha_2$, $\Delta\alpha_3$ and $\Delta\alpha_4$ the sine and cosine functions may be approximated into: $\sin\Delta\alpha_1 = \Delta\alpha_1$, $\sin\Delta\alpha_2 = \Delta\alpha_2$, $\sin\Delta\alpha_3 = \Delta\alpha_3$, $\sin\Delta\alpha_4 = \Delta\alpha_4$, $\cos\Delta\alpha_1 = \cos\Delta\alpha_2 = \cos\Delta\alpha_3 = \cos\Delta\alpha_4 = 1$. Accordingly the trigonometric functions of the angles α_1, α_2, α_3 and α_4 can be expressed in terms of $\Delta\alpha_1$, $\Delta\alpha_2$, $\Delta\alpha_3$, $\Delta\alpha_4$, sin α, cos α, sin β and cos β. Taking this method of approximation and also equations 9 and 10 into account the set of equations 32, 33, 35 and 37 can be linearized in the following form:

$$\Delta\alpha_1 = \frac{R'_\ell}{(R'_c + R'_\ell)} \frac{E'_c}{E'_m} \frac{1}{\cos\alpha} \tag{75}$$

$$\Delta\alpha_4 = \frac{R'_p}{R'_c} \frac{E'_c}{E'_m} \frac{1}{\cos\alpha} \tag{76}$$

$$(-4A'\omega \frac{B_s}{E'_m} - \cos\beta+\cos\alpha) \frac{\cos\alpha}{\sin\alpha} \Delta\alpha_1 + \frac{R'_\ell R'_c}{a} (\sin\alpha-\sin\beta)(\Delta\alpha_3+\Delta\alpha_2) = 0 \tag{77}$$

$$(\sin\alpha - \sin\beta)\left[\frac{2R'_\ell R'_c}{a} (\Delta\alpha_3 + \Delta\alpha_2) - \Delta\alpha_2\right] + (-4A'\omega \frac{B_s}{E'_m} -$$

$$- \cos\beta + \cos\alpha) \frac{\cos\alpha}{\sin\alpha} \Delta\alpha_1 = 0 \tag{78}$$

With the aid of equations 9 and 10 the simultaneous solution of equations 75 through 78 yields the set of equations 42 through 45.

APPENDIX II

The instantaneous value of the load current during the half cycle from α_1 to $\pi + \alpha_1$ as defined by equations 15, 19, 23 and 27 is

$$i'_\ell = \frac{-E'_c}{R'_c + R'_\ell} \qquad \alpha_1 \leq \omega t \leq \alpha_2$$

$$= \frac{R'_c}{a}\left(E'_m \sin \omega t - \ell' R'_p H_c - \frac{R'_p}{R'_c} E'_c\right) \qquad \alpha_2 \leq \omega t \leq \alpha_3$$

$$= 0 \qquad \alpha_3 \leq \omega t \leq \alpha_4$$

$$= \frac{R'_c}{a}\left(E'_m \sin \omega t + \ell' R'_p H_c - \frac{R'_p}{R'_c} E'_c\right) \qquad \alpha_4 \leq \omega t \leq \pi + \alpha_1 \qquad (79)$$

The load current waveform is such that it repeats itself every half a period of the excitation voltage. In other words the radian frequency of the load current function is equal to 2ω. Consequently the Fourier series expansion for the load current function can be written in the following form.

$$i'_\ell = \frac{A_o}{2} + \sum_{n=1}^{n=\infty} A_n \cos 2n\omega t + \sum_{n=1}^{n=\infty} B_n \sin 2n\omega t \qquad (80)$$

where

$$A_o = \frac{2}{\pi} \int_{\alpha_1/\omega}^{(\pi+\alpha_1)/\omega} i'_\ell \, dt$$

$$A_n = \frac{2}{\pi} \int_{\alpha_1/\omega}^{(\pi+\alpha_1)/\omega} i'_\ell \cos 2n\omega t \, dt$$

$$B_n = \frac{2}{\pi} \int_{\alpha_1/\omega}^{(\pi+\alpha_1)/\omega} i'_\ell \sin 2n\omega t \, dt$$

The evaluation of the coefficients of the Fourier series for the second harmonic component of the load current is obtained from equations 79 and 80.

$$A_o = 0 \tag{81}$$

$$A_1 = \frac{E'_c}{\pi(R'_c + R'_\ell)} [\cos 2\beta - \cos 2\alpha + 2(\beta-\alpha) \sin 2\beta] \tag{82}$$

$$B_1 = \frac{E'_c}{\pi(R'_c + R'_\ell)} [\sin 2\alpha - \sin 2\beta + 2(\beta-\alpha) \cos 2\beta] \tag{83}$$

The foregoing form of A_o, A_1 and B_1 was derived with the aid of equations 9, 35, 38 through 41 and 42 through 45.

The expression for the instantaneous value of the second harmonic current component may be written in the form

$$i'_2 = I'_{2a} \sin(2\omega t + \phi_2) \tag{84}$$

where

$$I'_{2a} = \sqrt{A_1^2 + B_1^2} \tag{85}$$

$$\phi_2 = \tan^{-1}\left(\frac{A_1}{B_1}\right) \tag{86}$$

Substituting equations 82 and 83 into equations 85 and 86 yields the expressions for I'_{2a} and ϕ_2 which are given by equations 48 and 49.

APPENDIX III

The rate of change of flux density in core II during the nonconduction interval can be found from equations 1 through 5 in the form

$$\frac{dB_{II}}{dt} = \frac{-1}{2A'}\left(E'_r - \ell' R'_p H_c\right) \tag{87}$$

Accordingly an expression for β can be obtained from the following condition

$$\int_0^{\beta/\omega} \frac{dB_{II}}{dt}\, dt = -2B_s \tag{88}$$

Substituting equation 87 into 88 and solving the integral yields equation 57.

NOMENCLATURE

A - effective core area; square centimeters.

B_I - instantaneous value of flux density in core I; gausses.

B_{II} - instantaneous value of flux density in core II; gausses.

B_s - saturation flux density; gausses.

e - instantaneous value of excitation voltage; volts.

E_m - maximum value of sinusoidal applied voltage; volts.

E_r - amplitude of rectangular alternating voltage; volts.

E_c - d.c. input voltage; volts.

H_I - instantaneous value of magnetizing force in core I; oersteds.

H_{II} - instantaneous value of magnetizing force in core II; oersteds.

H_c - dynamic coercive force, oersteds.

i_c - instantaneous value of current in the input circuit, amps.

i_ℓ - instantaneous value of current in the load circuit, amps.

i_p - instantaneous value of current in the excitation circuit, amp.

ℓ - length of magnetic circuit, centimeters.

N_c - number of turns per input winding.

N_ℓ - number of turns per load winding.

N_p - number of turns per excitation winding.

R_c - total resistance in input circuit, ohms.

R_ℓ - total resistance in load circuit, ohms.

R_p - total resistance in excitation circuit, ohms.

$e' = e/N_p$, $E'_m = E_m/N_p$, $E'_r = E_r/N_p$.

$i'_c = i_c N_c$, $i'_\ell = i_\ell N_\ell$, $i'_p = i_p N_p$.

$R'_c = R_c/N_c^2$, $R'_\ell = R_\ell/N_\ell^2$, $R'_p = R_p/N_p^2$.

$\ell' = \ell/0.4\pi$, $A' = A.10^{-8}$.

REFERENCES

1. L.Y. Lvov, "Transfer Function of Magnetic Amplifiers with Inductive Resistive Load" (in Russian), Automatika I Telemekhanika, No. 7, 1963.

2. F.C. Williams and S.W. Noble, "The Fundamental Limitations of the Second-Harmonic Type of Magnetic Modulator as Applied to the Amplification of Small D.C. Signals", Proceedings, Institution of Electrical Engineers, London, England, vol. 97, pt. II, pp. 445-59, 1950.

3. E.J. Kletsky, "Design Criteria for Low-Level Second-Harmonic Magnetic Modulators", AIEE Transactions, Vol. 77, pt. I, pp. 1013-19, 1958.

4. B.W. Jalbert, "An Analysis of the Operation of the Magnetic Second-Harmonic Modulator", Communication and Electronics, No. 49, pp. 268-272, July 1960.

5. K. Harada and S. Takeuchi, "Analysis of Peak-Height Magnetic Modulator", Electrical Engineering in Japan, Vol. 89, No. 2, 1969.